Using the linear sampling method and an improved maximum product criterion for the solution of the electromagnetic inverse medium problem

Fermín S.V. Bazán, Juliano B. Francisco, Koung Hee Leem, George Pelekanos

PII: S0377-0427(14)00273-8
DOI: http://dx.doi.org/10.1016/j.cam.2014.06.003
Reference: CAM 9697

To appear in: *Journal of Computational and Applied Mathematics*

Received date: 9 September 2013
Revised date: 16 April 2014

Please cite this article as: F.S.V. Bazán, J.B. Francisco, K.H. Leem, G. Pelekanos, Using the linear sampling method and an improved maximum product criterion for the solution of the electromagnetic inverse medium problem, *Journal of Computational and Applied Mathematics* (2014), http://dx.doi.org/10.1016/j.cam.2014.06.003

Using the linear sampling method and an improved maximum product criterion for the solution of the electromagnetic inverse medium problem

Fermín S. V. Bazán [1]*, Juliano B. Francisco[1],
Koung Hee Leem [2] and George Pelekanos [2]
[1] Department of Mathematics Federal University of Santa Catarina
Florianópolis SC, Santa Catarina, CEP 88040-900, Brazil
[2] Department of Mathematics and Statistics, Southern Illinois University,
Edwardsville, IL 62026, USA
E-mail: fermin@mtm.ufsc.br, juliano@mtm.ufsc.br,
kleem@siue.edu and gpeleka@siu.edu

Abstract

We present a Tikhonov parameter choice approach for three-dimensional reconstructions based on a maximum product criterion (MPC) which provides a regularization parameter located in the concave part of the L-curve in log-log scale. Our method, baptised Improved Maximum Product Criterion (IMPC), is an extension of the MPC method developed by Bazán et al for two-dimensional reconstructions. In the 3D framework, IMPC computes the regularization parameter via a fast iterative algorithm and requires no *a priori* knowledge of the noise level in the data. It is applied on the linear sampling method for solving the electromagnetic inverse medium problem in the 3D framework. The effectiveness of IMPC is illustrated with numerical examples involving more than one scatterer.

1 Introduction

In this work we shall consider the scattering of a time harmonic electromagnetic wave with frequency in the resonance region by a finite number of three dimensional scatterers each of which is a penetrable isotropic medium. The inverse scattering problem we are considering is related to the determination of the shape of a penetrable scatterer in $\mathbb{R}^3$.

*The research of this author is supported by CNP, Brazil, grants 3087909/2011-0, 477093/2011-6

The approach we shall use to solve the inverse electromagnetic scattering problem is a combination of the well known linear sampling method originally developed in the acoustic context by Colton and Kirsch [5] and an improved version of the maximum product criterion (MPC) developed by Bazán et al [4] for 2D reconstructions. It is widely known that the linear sampling method does not require *a priori* information about either the boundary condition or the connectivity of the scatterer, however it does require multistatic data at a single frequency. Due to the ill-posedness of the inverse problem, the linear sampling method yields an ill-conditioned system of linear equations whose solution requires a regularization method in order to handle correctly the presence of noise in the data. In particular, this solution requires the use of Tikhonov regularization method equipped with Morozov's generalized discrepancy principle as parameter choice rule [1, 5, 7, 8, 9, 10, 11], which generally involves the computation of the zeros of the discrepancy function at each point of the grid. In addition, the noise level in the data should be known *a priori*, something that in real life applications is not the case in general.

For electromagnetism, the linear sampling method has already been analysed for perfect conducting scatters [16], imperfect conductors with impedance boundary data [10] and penetrable scatterers [13]. In particular, as presented in [13], the mathematical justification of the method is based on the formulation of an interior transmission problem for which a weak solution is shown to exist. Then the theoretical justification follows by extending to electromagnetics methods used for the acoustic problem.

The Maximum Product Criterion (MPC), originally developed for two dimensional reconstructions [4], employs computation of the regularized solution norm and the corresponding residual norm and selects the parameter which maximizes the product of these norms as a function of the regularization parameter; its main virtue is that it constructs regularized solutions of either large or small norm depending on whether a certain inclusion condition is satisfied or not. MPC however applied to 3D reconstruction problems may fail due to the existence of several local maxima. To overcome this difficulty the authors developed a variant of MPC, the Improved Product Criterion (IMPC), which via a fast and efficient algorithm chooses as regularization parameter the critical point associated with the largest local maximum of the product. In addition as with MPC, IMPC does not depend on user specified input parameters (like subspace dimension or truncating parameter) and requires no *a priori* knowledge of the noise level.

We organize our paper as follows. Section 2 will be devoted to the formulation of the problem and a brief description of the linear sampling method in the electromagnetic context. Subsequently, Section 3 will deal with the improved version of MPC, the IMPC as a parameter choice rule. In particular we will be concerned with theoretical properties on which IMPC relies on as well as with its implementation within the framework of the linear sampling method. In order to show the effectiveness of our method, in Section 4, we will present numerical examples for the case of penetrable three dimensional scatterers and we will compare the reconstructions obtained via IMPC with the ones obtained by means of the Morozov's generalized discrepancy principle (GDP). We will finally list our conclusions in Section 5.

2 The linear sampling method

We begin by considering the direct scattering problem of a time harmonic electromagnetic wave by a penetrable isotropic medium $D \subset \mathbb{R}^3$ which can be formulated as the problem of finding an electric field E and a magnetic field H such that $E, H \in C^1(\mathbb{R}^3)$ and

$$\text{curl}E - ikH = 0 \;\; and \;\; \text{curl}H + iknE = 0 \;\; in \; \mathbb{R}^3 \tag{1}$$

where $n \in C^{1,\alpha}(\mathbb{R}^3)$ is a complex valued function with $0 \leq \alpha \leq 1$ and $n(x) = 1$ outside D. The total field is given as

$$E = E^i + E^s \;\; and \;\; H = H^i + H^s \tag{2}$$

where E^s, H^s is the scattered field satisfying the Silver-Müller radiation condition

$$\lim_{r\to\infty}(H^s \times x - rE^s) = 0 \tag{3}$$

uniformly in $\hat{x} = \frac{x}{|x|}$, where $r = |x|$ and the incident field is the plane wave

$$E^i(x) = \frac{i}{k}\text{curlcurl}\, pe^{ikx\cdot d} = ik(d \times p) \times de^{ikx\cdot d}, \tag{4}$$

$$H^i(x) = \text{curl}\, pe^{ikx\cdot d} = ikd \times pe^{ikx\cdot d}, \tag{5}$$

where the wavenumber k is positive, d is a unit vector giving the direction of propagation and p is the polarization vector. The existence and uniqueness of a solution to (1)-(3) can be found in [6]. From the second Stratton-Chu formula it follows that

$$E^s(x) = \frac{e^{ikr}}{r}\left\{E_\infty(\hat{x}, d, p) + O(\frac{1}{r})\right\} \;\; \text{as } r \to \infty \tag{6}$$

where E_∞ is the electric far field pattern. The inverse medium problem for electromagnetic waves is to determine D from $E_\infty(\hat{x}, d, p)$ for $\hat{x}$, d in the unit sphere Ω, $p \in \mathbb{R}^3$, and different values of k. As indicated in [13], E_∞ is infinitely differentiable as a function of its arguments and as a function of $\hat{x}$ is tangential to the unit sphere Ω.

We now introduce the space

$$L_t^2(\Omega) = \{g : \Omega \to \mathbb{C}^3 |\, g \in L^2(\Omega), \;\; g \cdot \hat{x} = 0, \text{ for } \hat{x} \in \Omega\}$$

of tangential L^2 fields in Ω. The electric far-field operator $\mathcal{F} : L_t^2(\Omega) \to L_t^2(\Omega)$ is then defined by

$$(\mathcal{F}g)(\hat{x}) = \int_\Omega E_\infty(\hat{x}, d, g(d))\, ds(d), \quad \hat{x} \in \Omega \tag{7}$$

Now let $E_\infty(\hat{x}, z, q)$ be the electric far-field pattern of an electric dipole located in $z \in D$ and oriented along q:

$$E_e(x, z, q) = \frac{i}{k}\text{curl}_x\text{curl}_x q\Phi(x, z) \tag{8}$$

$$H_e(x, z, q) = \text{curl}_x q\Phi(x, z) \tag{9}$$

with Φ being the fundamental solution of the Helmholtz equation defined by

$$\Phi(x,z) = \frac{1}{4\pi}\frac{e^{ik|x-z|}}{|x-z|}. \tag{10}$$

We would like to find for fixed q and z, a function $g(\cdot,z,q) \in L_t^2(\Omega)$ through the far-field equation

$$(\mathcal{F}g(\cdot,z,q))(\hat{x}) = \int_\Omega E_\infty(\hat{x},d,g_{z,q}(d))\,ds(d) = E_{e,\infty}(\hat{x},z,q) \tag{11}$$

where $E_{e,\infty}(\hat{x},d,g_{z,q}(d))$ denotes the far-field pattern of E_e which is the field scattered by the target along direction $\hat{x}$ when is illuminated by a plane wave impinging from the direction d and polarized along $g_{z,q}(d) \in L_t^2(\Omega)$ for a set of sampling points $z \in \mathbb{R}^3$, three linear independent polarizations $q \in \mathbb{R}^3$ and

$$E_{e,\infty}(\hat{x},z,q) = \frac{ik}{4\pi}(\hat{x}\times q)\times \hat{x}e^{-ik\hat{x}\cdot z}. \tag{12}$$

It can be shown [13], that the existence of a solution to (11) is equivalent to the existence of a solution of an appropriate electromagnetic interior transmission problem. In [13] it was shown that the far field equation (11) has a nearby solution $g_{\epsilon,z,q}(\cdot)$, where *epsilon* can be interpreted as the noise level in the far-field operator, such that the L^2 norm of this solution becomes unbounded as z approaches the boundary. Furthermore, if z is outside D, there exists a nearby regularized solution $g^\delta_{\epsilon,z,q}(\cdot)$ (which corresponds to a noise level equal to $\epsilon+\delta$) such that the L^2 norm of this solution becomes unbounded as δ approaches 0. The observations above are summarized in the following theorem whose proof can be found in [13].

Theorem 2.1 *Let q be any element of in $\mathbb{R}^3$ and the index of refraction n satisfies some regularity conditions given in theorem 3.1 of [13]. Then we have*
(a) if $z \in D$, then for every $\epsilon > 0$ there exists a solution $g_\epsilon(\cdot,z,q) \in L^2(\Omega)$ of the inequality

$$||\mathcal{F}g_\epsilon(\cdot,z,q) - E_{e,\infty}(\cdot;z,q)||_{L^2(\Omega)} \leq \epsilon \tag{13}$$

such that

$$\lim_{z\to\partial D} ||g_\epsilon(\cdot,z,q)||_{L^2(\Omega)} = \infty; \tag{14}$$

(b) if $z \notin D$, then for every $\epsilon > 0$ and $\delta > 0$ there exists a solution $g^\delta_\epsilon(\cdot,z,q) \in L^2(\Omega)$ of the inequality

$$||\mathcal{F}g^\delta_\epsilon(\cdot,z,q) - E_{e,\infty}(\cdot;z,q)||_{L^2_t(\Omega)} \leq \epsilon+\delta \tag{15}$$

such that

$$\lim_{\delta\to 0} ||g^\delta_\epsilon(\cdot,z,q)||_{L^2(\Omega)} = \infty; \tag{16}$$

Based on Theorem 2.1 and on the fact that the far field equation is ill-posed as the far field operator is compact [10, 8, 13], the linear sampling method suggests that to determine the

boundary of D from the far field pattern $E_\infty(\hat{x}, d, g(d))$, for each point z in a grid containing the scatterer and a fixed $q \in \mathbb{R}^3$, one should solve the far field equation (11) using Tikhonov regularization for $g_\lambda(\cdot, z, q)$. This done, the boundary ∂D is determined by looking for those z for which the norm $\|g_\lambda(\cdot, z, q)\|^2$ is large. We emphasize that regularization is necessary when solving the far field equation as in practice the integral operator is affected by measurement noise. As far as the choice of Tikhonov regularization parameter is concerned, it has been done by the Generalized discrepancy principle (GDP) [10, 8, 13] which requires knowledge of estimates of the noise level in the data. As an alternative to GDP, Bazán et al [4] have developed a new criterion called MPC which does not require any knowledge of the noise level; both parameter choice rules can fail in some circumstances.

3 Improvements to the maximum product criterion algorithm for the selection of the Tikhonov parameter

In practice the far-field equation must be discretized in order to construct approximate solutions to the continuous problem. However, the main difficulty associated to this construction process is that since the original problem is ill-posed, its finite dimensional counterpart is ill-conditioned and characterized by numerical instability. As a result, the approximate solution becomes less and less reliable as the quality of the discretization improves and regularization is necessary to construct stable approximations. In what follows we assume that the unit sphere is discretized using a triangular mesh containing N vertices (which are also used as directions for the plane incident waves) and that the far-field equation is discretized by following the scheme described in [8]. This gives rise to a system of $2N \times 2N$ linear equations which we refer to as the discrete far-field equation

$$F g_z = r_{z,q}, \qquad F \in \mathbb{C}^{2N \times 2N} \tag{17}$$

where $r_{z,q} \in \mathbb{C}^{2N}$ is a discrete counterpart of $E_{e,\infty}(\cdot; z, q)$ and F denotes the far-field matrix. In practice only a noisy far-field matrix is available and assumed to be of the form $\widetilde{F} = F + E$, with E being introduced to denote measurement noise. Since the discrete far-field equation is ill-conditioned, Tikhonov regularization has been used to compute stable approximate solutions with the regularization parameter being chosen by the generalized discrepancy criterion. Tikhonov regularization applied to the discrete far-field equation yields regularized solutions defined by

$$g_{\lambda,z} = \operatorname{argmin}_{g \in \mathbb{C}^{2N}} \{\|r_{z,q} - \widetilde{F}\, g\|_2^2 + \lambda^2 \|g\|_2^2\} \tag{18}$$

where $\lambda > 0$ is the regularization parameter. GDP chooses as regularization parameter the only root of the nonlinear equation

$$G(\lambda) = \|r_{z,q} - \widetilde{F}\, g_{\lambda,z}\|_2^2 - \delta_A^2 \|g_{\lambda,z}\|_2^2 = 0 \tag{19}$$

where δ_A is an estimate for $\|E\|$ such that $\|E\| \leq \delta_A$. GDP works well when $\|E\|$ is accurately estimated but this may not be the case in real life applications. There exist some alternative

parameter selection criteria that avoid knowledge of the noise level, referred to as heuristic parameter choice rules, which have also been used in inverse scattering; these include L-curve [14, 18] and a Fixed-point method [2, 17]. Recently, Fares et al [12] developed a new heuristic algorithm, the SVD-tail, based on the combined presence of error in the operator and eigenvalue clusters corresponding to a singular subspace associated with a few small singular values. SVD-tail is proven efficient since the point-wise solution of the far-field equation is never explicitly constructed; one of its disadvantages though is that the quality of the reconstruction depends on the chosen dimension of the singular subspace.

More recently, Bazan et al [4] introduced the so-called maximum product criterion (MPC) which defines as regularization parameter a solution to the problem

$$\lambda^* = \text{argmax}\{\, \Psi(\lambda)\,\}, \qquad \Psi(\lambda) = \mathbf{x}(\lambda)\,\mathbf{y}(\lambda), \tag{20}$$

where

$$\mathbf{y}(\lambda) = \|g_{\lambda,z}\|^2, \qquad \mathbf{x}(\lambda) = \|r_{z,q} - \widetilde{F} g_{\lambda,z}\|_2^2. \tag{21}$$

Existence of maximum is always guaranteed when the far field matrix is non singular as Ψ is positive and

$$\Psi(0) = 0 = \lim_{\lambda\to\infty} \Psi(\lambda). \tag{22}$$

The main virtue of MPC (illustrated on 2D reconstruction problems in [4]) is that it delivers regularized solutions of large norm for z outside D and regularized solutions of small norm for z inside, a necessary condition for LSM to produce good reconstructions. From the practical point of view, under the assumption that Ψ has a unique maximizer, the authors in [4] show that such a maximizer is the only non zero root of the function

$$\varphi(\lambda) = \mathbf{x}(\lambda) - \lambda^2 \mathbf{y}(\lambda) = 0 \tag{23}$$

and that this root can be computed by using some root finder such as the regula falsi method or other. However, we realize when solving 3D reconstruction problems that MPC can fail when the function Ψ has several local maxima. Difficulties arise since, depending on factors such as the chosen root finder, the chosen initial guess, etc., the regularization parameter determined in this way may not be suitable to ensure the success of LSM.

3.1 An improved version of MPC

First of all we note that extreme points of Ψ are fixed points of the function ϑ defined by

$$\vartheta(\lambda) = \frac{\|r_{z,q} - \widetilde{F} g_{\lambda,z}\|}{\|g_{\lambda,z}\|}, \quad \lambda > 0, \tag{24}$$

or equivalently roots of function φ as seen from (23). Using the fact that the regularized solution norm and the corresponding residual norm are monotone, see, e.g., [4], it follows that ϑ is an increasing function of λ and therefore no local maximum of Ψ can be computed by using fixed point iterations of the form $\lambda_{k+1} = \vartheta(\lambda_k),\ k \geq 0$. This is explained by the fact that depending on the chosen initial guess, either the iterations converge to a minimum

of Ψ or to the value $\lambda = 0$, or the iterations diverge to infinity. As an example, assume that λ_0 is such that $\vartheta(\lambda_0) < \lambda_0$. When this is the case, either $\{\lambda_k\}$ converges to 0 if ϑ does not have a non zero fixed point located to the left of λ_0 as $\{\lambda_k\}$ is a decreasing sequence, or $\{\lambda_k\}$ converges to a non zero fixed point located to the left of λ_0. This can be better interpreted from the behavior of a function ϑ as seen in Fig. 1.

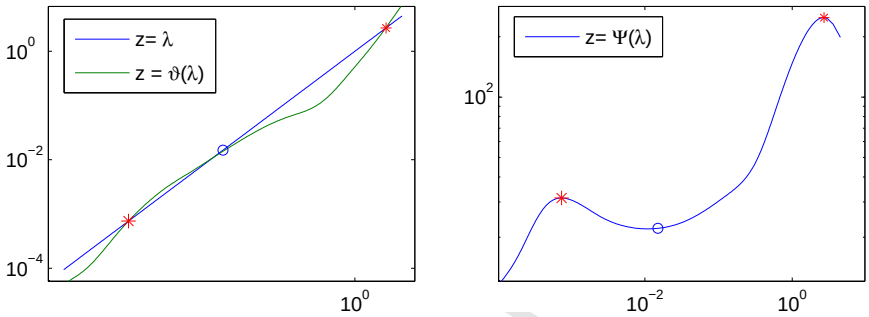

Figure 1: Typical behavior of function ϑ with several fixed points and function Ψ with several critical points. Maximum points are marked with star.

Another difficulty with MPC when the function Ψ has several local maxima is how to choose one of them. Aiming at avoiding these difficulties, we propose

i) to choose as regularization parameter the largest maximum local of Ψ

ii) a fast algorithm to compute the regularization parameter.

The following theorem provides information on the largest maximizer of Ψ in terms of the singular value decomposition (SVD) of the far-field matrix $\widetilde{F}$. For latter use, recall that the SVD of $\widetilde{F}$ is of the form

$$\widetilde{F} = U\Sigma V^* \tag{25}$$

where $U = [u_1, \ldots, u_{2N}]$, $V = [v_1, \ldots, v_{2N}]$ are orthonormal matrices, and $\Sigma = \mathrm{diag}(\sigma_1, \ldots, \sigma_{2N})$, with $\sigma_1 \geq \sigma_2 \geq \cdots \geq \sigma_{2N}$.

Theorem 3.1 *Let the far-field matrix $\widetilde{F}$ have the SVD (25). Assume that $\widetilde{F}$ is nonsingular and that its singular values are distinct. Then the following assertions hold*

a) *function Ψ has at least one critical point inside (σ_{2N}, σ_1) and at most one critical point inside $(\frac{\sqrt{3}}{3}\sigma_1, \sigma_1)$.*

b) *function Ψ has a maximum at $\lambda = \widehat{\lambda}$ if and only if $\varphi(\widehat{\lambda}) = 0$ and $\vartheta'(\widehat{\lambda}) > 1$ where φ and ϑ are introduced in (23) and (24), respectively.*

Proof: Using the SVD of $\widetilde{F}$ and (21) we have

$$\mathbf{x}(\lambda) = \sum_{i=1}^{2N} \frac{\lambda^4 \alpha_i}{(\sigma_i^2 + \lambda^2)^2}, \quad \mathbf{y}(\lambda) = \sum_{i=1}^{2N} \frac{\sigma_i^2 \alpha_i}{(\sigma_i^2 + \lambda^2)^2}. \tag{26}$$

where $\alpha_i = |u_i^* r_{z,q}|^2$. Therefore

$$\varphi(\lambda) = \mathbf{x}(\lambda) - \lambda^2 \mathbf{y}(\lambda) = \sum_{j=1}^{2N} \frac{\lambda^2(\lambda^2 - \sigma_i^2)\alpha_i}{(\sigma_i^2 + \lambda^2)^2}.$$

From this we see that $\varphi(\lambda) \geq 0$ if $\lambda \geq \sigma_1$ and $\varphi(\lambda) \leq 0$ if $\lambda \leq \sigma_{2N}$. We also see that σ_1 (respectively σ_{2N}) cannot be a root of φ since by assumption all singular values are distinct. This implies that φ must have at least a root inside the interval (σ_{2N}, σ_1) or equivalently that Ψ has at least a critical point inside (σ_{2N}, σ_1) as the critical points of Ψ are roots of φ [4]. We now see that

$$\mathbf{x}'(\lambda) = 4\lambda^3 \sum_{i=1}^{2N} \frac{\sigma_i^2 \alpha_i}{(\sigma_i^2 + \lambda^2)^3} > 0, \quad \mathbf{y}'(\lambda) = -4\lambda \sum_{i=1}^{2N} \frac{\sigma_i^2 \alpha_i}{(\sigma_i^2 + \lambda^2)^3} < 0. \tag{27}$$

Hence, the derivative of φ with respect to λ becomes

$$\begin{aligned} \varphi'(\lambda) &= \mathbf{x}'(\lambda) - 2\lambda \mathbf{y}(\lambda) - \lambda^2 \mathbf{y}'(\lambda) \\ &= -2[\lambda \mathbf{y}(\lambda) + \mathbf{x}'(\lambda)] = -2 \sum_{j=1}^{2N} \frac{\lambda \sigma_i^2 (3\lambda^2 - \sigma_i^2)\alpha_i}{(\sigma_i^2 + \lambda^2)^3}. \end{aligned}$$

This shows that $\varphi'(\lambda)$ does not change sign inside $(\frac{\sqrt{3}}{3}\sigma_1, \sigma_1)$. Thus, if Ψ has a critical point inside this interval, this critical point is unique and the proof of item a) is complete. To prove assertion b) observe from (23) that $\widehat{\lambda}$ is a critical point of Ψ if and only if $\varphi(\widehat{\lambda}) = 0$, this being true if and only if $\vartheta(\widehat{\lambda}) = \widehat{\lambda}$. Now a simple calculation gives

$$\Psi''(\lambda) = [-2\lambda + 2\vartheta(\lambda)\vartheta'(\lambda)]\mathbf{y}(\lambda)\mathbf{y}'(\lambda) + [-\lambda^2 + \vartheta^2(\lambda)][\mathbf{y}(\lambda)\mathbf{y}'(\lambda)]'. \tag{28}$$

This shows that at $\lambda = \widehat{\lambda}$ we have $\Psi''(\widehat{\lambda}) < 0 \quad \text{iff} \quad \vartheta'(\widehat{\lambda}) > 1$, and assertion b) is proved. □

The assumption that all singular values are distinct and positive is very natural when the noisy far-field matrix comes from a random perturbation of the exact far-field matrix. When this is the case, condition (22) is insured and so function ϑ has a fixed point that maximizes Ψ. For a discussion regarding existence of fixed points of ϑ for the case where the coefficient matrix is singular or rank-deficient and rectangular, the reader is referred to [2, 3]. Regarding the consequences of Theorem 3.1, notice from assertion b) that maximizers of Ψ are fixed points of ϑ such that $(\vartheta(\lambda) - \lambda)$ changes sign from negative to positive as λ increases in a vicinity of the fixed points, see Fig. 1. In such case the largest fixed point of ϑ corresponds to the largest local maximum of Ψ, as is illustrated for a typical function ϑ in inverse scattering, see Figure 1 again.

The following theorem shows how to use the previous theorem in order to develop an algorithm for computing the largest maximizer of Ψ.

Theorem 3.2 *For fixed z and $\lambda > 0$ consider the function $\xi : \mathbb{R}^+ \mapsto \mathbb{R}^+$ defined by*

$$\xi(\lambda) = \frac{\lambda^2}{\vartheta(\lambda)}. \tag{29}$$

Then ξ increases as λ increases and $\xi(\lambda) \leq \sigma_1$ $\forall \lambda > 0$. Further, consider the sequence

$$\lambda_{k+1} = \xi(\lambda_k), \quad k \geq 0. \tag{30}$$

Then λ_k converges monotonically to the largest fixed point of ξ (hence to the largest fixed point of ϑ) as long as the initial guess λ_0 is chosen in the interval $[\frac{\sqrt{3}}{3}\sigma_1, \sigma_1]$.

Proof: Since $\xi(\lambda)\vartheta(\lambda) = \lambda^2$, differentiation with respect to λ yields

$$\xi(\lambda)\vartheta'(\lambda) + \xi'(\lambda)\vartheta(\lambda) = 2\lambda,$$

and therefore

$$\xi'(\lambda)\vartheta(\lambda) = \frac{2\lambda\vartheta(\lambda) - \lambda^2\vartheta'(\lambda)}{\vartheta(\lambda)}. \tag{31}$$

Now let $\mathbf{x}(\lambda) = \rho^2(\lambda)$ and $\mathbf{y}(\lambda) = \eta^2(\lambda)$. Then it follows that

$$\mathbf{x}'(\lambda) = 2\rho(\lambda)\rho'(\lambda), \quad \mathbf{y}'(\lambda) = 2\eta(\lambda)\eta'(\lambda), \tag{32}$$

and thus

$$\frac{d\mathbf{y}}{d\mathbf{x}} = \frac{1}{\vartheta}\frac{d\eta}{d\rho} \Leftrightarrow \frac{d\eta}{d\rho} = -\frac{\vartheta(\lambda)}{\lambda^2},$$

where the last equality is because of (27). Taking derivative with respect to λ on the right equality leads to

$$\frac{d^2\eta}{d\rho^2}\rho'(\lambda) = \frac{2\lambda\vartheta(\lambda) - \lambda^2\vartheta'(\lambda)}{\lambda^4}$$

Since $\rho'(\lambda) > 0$ by (32) and (27), and since η is a convex decreasing function of ρ, see, e.g., [14, Theorem 4.6.1], combining the last equality with (31) it follows that $\xi'(\lambda) > 0$. This proves that ξ increases with λ. Now notice that function ξ can be rewritten as

$$\xi(\lambda) = \sqrt{\sum_{i=1}^{2N} \frac{\sigma_i^2\alpha_i}{(\sigma_i^2 + \lambda^2)^2}} \Bigg/ \sqrt{\sum_{i=1}^{2N} \frac{\alpha_i}{(\sigma_i^2 + \lambda^2)^2}} \tag{33}$$

from which the inequality $\xi(\lambda) \leq \sigma_1$ readily follows.

Proceeding with the proof, we now notice that $\widehat{\lambda}$ is a fixed point of ϑ if and only if $\widehat{\lambda}$ is a fixed point of ξ. Notice also that the curve $(\lambda, \xi(\lambda))$ lies below the constant line $z = \sigma_1$, as illustrated in Fig. 2. Hence, if ξ has a fixed point inside $[\frac{\sqrt{3}}{3}\sigma_1, \sigma_1]$ and the initial guess λ_0 is chosen in this interval, the sequence $\{\lambda_k\}$ will converge to that fixed point of ξ as $\{\lambda_k\}$ is monotone due to ξ being an increasing function. A similar argument holds true if the largest fixed point of ξ does not belong to $(\frac{\sqrt{3}}{3}\sigma_1, \sigma_1)$. This concludes the proof. □

We now transform the theoretical results of Theorem 3.2 into a practical algorithm. To this end we notice that as we already know the sequence $\{\lambda_k\}$ converges to the largest fixed point of ϑ (which hopefully maximizes Ψ), what remains to do is to introduce a test to ensure that the captured fixed point actually maximizes Ψ. This gives rise to a new algorithm which we refer to as IMPC and we describe as follows.

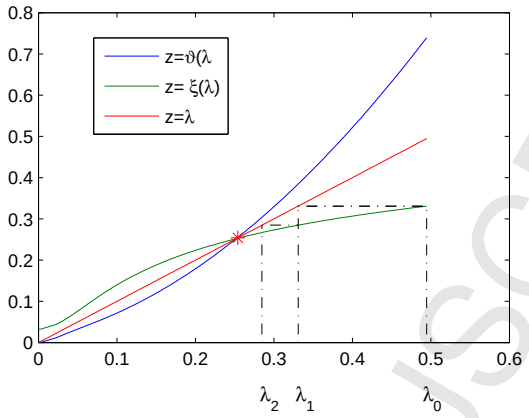

Figure 2: Typical behavior of functions $\Phi(\lambda)$, $\xi(\lambda)$ and the sequence $\{\lambda_k\}$ when initialized as in Theorem 3.2. In this illustration the initial guess is taken to be $\lambda_0 = \sigma_1$. The largest fixed point of ξ is marked with star.

Improved version of MPC algorithm (IMPC)

Input: σ_1, *tol*

1. Set $k = 0$ and choose λ_0 in the interval $[\frac{\sqrt{3}}{3}\sigma_1, \sigma_1]$
2. Compute $s_0 = \xi(\lambda_0)/\lambda_0$.
3. **while** $(|s_k - 1| > tol\ )$ **do**
   $\lambda_{k+1} = \xi(\lambda_k), \quad s_k = \lambda_{k+1}/\lambda_k$
   $k = k + 1$
   end while
4. **if** $(\vartheta'(\lambda_k) > 1)$ **do**
   $\lambda^* = \lambda_k$
   elseif $(\ \vartheta'(\lambda_k) = 1)$ **do**
   Set $k = 0$, $\lambda_0 = 0.9 * \lambda_k$, and go to step 2
   end if

Remark: The improved version of MPC can also be implemented in conjunction with Kirsch's method: it suffices to replace σ_i^2 by σ_i in (33).

As a consequence of the analysis above we now show that the regularization parameter chosen by the generalized discrepancy principle can also be determined by a fixed point iteration algorithm. This is the subject of the following theorem.

Theorem 3.3 *For fixed z and $\lambda > 0$ consider the function $\zeta : \mathbb{R}^+ \mapsto \mathbb{R}^+$ defined by*

$$\zeta(\lambda) = \frac{\lambda\sqrt{\delta_A}}{\sqrt{\vartheta(\lambda)}}. \tag{34}$$

Let $\{\lambda_k\}$, $k \geq$ be the sequence defined by

$$\lambda_{k+1} = \zeta(\lambda_k),\ k \geq 0. \tag{35}$$

Assume that $\delta_A < \sigma_1$. Then $\{\lambda_k\}$ converges globally and monotonically to the regularization parameter chosen by GDP irrespective of the initial guess chosen.

Proof: Based on the SVD of $\widetilde{F}$ (25) and (26), the discrepancy equation (19) reads

$$G(\lambda) = \sum_{j=1}^{2N} \frac{(\lambda^4 - \delta_A^2 \sigma_i^2)\alpha_i}{(\sigma_i^2 + \lambda^2)^2} = 0. \tag{36}$$

Then function G is increasing due to (27) and has a unique root when $\delta_A < \sigma_1$. But $G(\lambda) = 0$ is equivalent to $\frac{\delta_A}{\vartheta(\lambda)} = 1$, and this implies that $G(\lambda) = 0$ has a unique root if and only if this root is a non zero fixed point of ζ. Now it is not difficult to check that

$$\lim_{\lambda \to 0} \zeta(\lambda) = K > 0$$

for appropriate constant K and that for $\lambda > \sigma_1$ we have $\zeta(\lambda) < \lambda$. Taking into account the results of the above analysis and since $\zeta = \sqrt{\delta_A}\sqrt{\xi}$ increases with λ, as ξ so does, we deduce that the sequence (35) is monotone and the assertion of the theorem follows. □

Similar to the MPC case, we can now transform the results of Theorem 3.3 into a practical fixed point algorithm for determining the Tikhonov regularization parameter chosen by GDP. We refer to this algorithm as FP-GDP; it can be outlined as follows.

Fixed point approach for GDP (FP-GDP)

Input: σ_1, *tol*

1. Set $k = 0$ and choose $\lambda_0 \approx \sigma_1$
2. Compute $s_0 = \zeta(\lambda_0)/\lambda_0$.
3. **while** $(|s_k - 1| > tol\ )$ **do**
   $\lambda_{k+1} = \zeta(\lambda_k), \quad s_k = \lambda_{k+1}/\lambda_k$
   $k = k + 1$
   end while

Our experience in terms of computational time spent by FP-GDP and IMPC when applied to 2D reconstruction problems is that both are efficient and fast but with a slight advantage in favor of the former. Now, when comparing them to an implementation of GDP coupled with regula falsi as root finder, our experience is that FP-GDP and IMPC are significantly faster. As an example, Table 1 displays the time spent by these algorithms in solving a 2D reconstruction problem involving a far field matrix of size 32×32 for each z in a grid of 2500 points.

Table 1: Time spent (in seconds) by an implementation of GPP with regula falsi as root finder (denoted here by RF-GDP), FP-GDP and IMPC

	RF-GDP.	FP-GDP	IMPC
t(sec.)	20.3253	0.9457	1.2143

4 Numerical Applications

In this paper we will not present details of the discretization of equation (11) since we used the approach presented in [10]. Instead we describe two examples in which the discrete solution is computed using the Tikhonov regularization method where the regularization parameter is chosen by the new version of MPC designed for 3D reconstruction problems. Comparison with Morozov's discrepancy principle (GDP) takes place and hence the effectiveness of the IMPC is illustrated. In both examples we corrupt the exact far-field matrix F with noise

$$\widetilde{F} = F + \epsilon \|F\| \mathcal{N},$$

where $\mathcal{N}$ is a random noise matrix normalized such that $\|\mathcal{N}\|_2 = 1$ and ϵ is an error parameter. The numerical experiments use synthetic data that have been created by CESC. CESC is a solver for electromagnetic scattering problems developed at CERFACS. In [8] has been explained that the best reconstruction is obtained by combining three different inverse resolutions corresponding to $q = q_1, q_2$ and q_3 for the right hand side $E_{\epsilon,\infty}$, where (q_1, q_2, q_3) is an orthogonal basis of $\mathbb{R}^3$. Hence as in [8, 13] our algorithm is based on the evaluation of

$$W(z) = \frac{1}{3}\left(\|g(\cdot, z, q_1)\|^{-1} + \|g(\cdot, z, q_2)\|^{-1} + \|g(\cdot, z, q_3)\|^{-1}\right). \tag{37}$$

where $q_1 = (1, 0, 0)$, $q_2 = (0, 1, 0)$ and $q_3 = (0, 0, 1)$. To this end we consider a uniform grid in a box containing the object and denote by $\mathcal{Z}$ the set of all these grid points. As discussed before $\|g(\cdot, z, q)\|$ becomes arbitrarily large when z approaches the boundary from inside and remains large when z is outside. The reconstruction is then visualized by plotting the isosurface

$$\mathcal{S} = \{z \in \mathcal{Z} \mid W(z) = \tau\},$$

for an isovalue parameter τ such that the level set $\mathcal{S}$ is a suitable visual representation of the unknown object. The isovalue parameter can be selected by trial and error or based on heuristics. Among several ways to choose the isovalue parameter, two parameter choices stand out. The first, very popular in the last decade (see, e.g. [9, 10, 8, 13]), defines the isovalue parameter as

$$\tau_1 = C \max_{z \in \mathcal{Z}} W(z) \tag{38}$$

with C chosen close to zero (e.g., 0.3 , 0.2 , etc) or with C varying until the "best" reconstruction is obtained, and the second, due to Fares et al [12], based on elementary statistics and referred to as the global mean and standard deviation (GMSD) heuristic, which defines the isovalue parameter as

$$\tau_2 = \operatorname*{mean}_{z \in \mathcal{Z}} [W(z)] + 2 \operatorname*{std}_{z \in \mathcal{Z}} [W(z)]. \tag{39}$$

As indicated in [8, 13], in practice it is difficult to know how to choose C since g is computed from noisy data. Hence, automated reconstructions based on (38) can fail when the isovalue parameter is too small; a similar comment applies to the GMSD heuristic. Numerical illustrations that confirm this observation are postponed to Subsection 4.2.

In all our numerical experiments the reconstructed object is visualized using Matlab's isosurface function with the isovalue parameter being defined by

$$\tau_{\text{IMPC}} = \min_{z \in \mathcal{Z}} W(z) + \tau \left[\max_{z \in \mathcal{Z}} W(z)) - \min_{z \in \mathcal{Z}} W(z)\right]. \quad 0 < \tau < 1. \tag{40}$$

Our proposal relies on the observation that what really matters here is to find an isosurface $\mathcal{S}$ associated with large values of $W(z)$. Based on this, we use $\tau \approx 0.5$, which was found to produce good reconstructions in our experiments. All the numerical reconstructions are performed by using 92 uniformly distributed nodes on Ω, which means the far-field matrix $\widetilde{f}$ is 184×184, far fielda uniform grid for $z \in [-2, 2]^3$ with mesh step $4/60$, a wavenumber $k = 3$ and, except for the last example, the noise level is $\epsilon = 0.01$. In all examples the far-field matrix $\widetilde{F}$ is 184×184 and all quantities required by the IMPC algorithm are computed by using the SVD of $\widetilde{F}$.

4.1 Example 1

In this example the exact scatterer is an ellipsoid, centered at the origin (not shown here) which is made of a homogeneous absorbing material: $n(x) = 2 + 2i$. The isolines of W for different cross sections are shown in figure 3 and provide a good indicator of the shape of the scatterer.

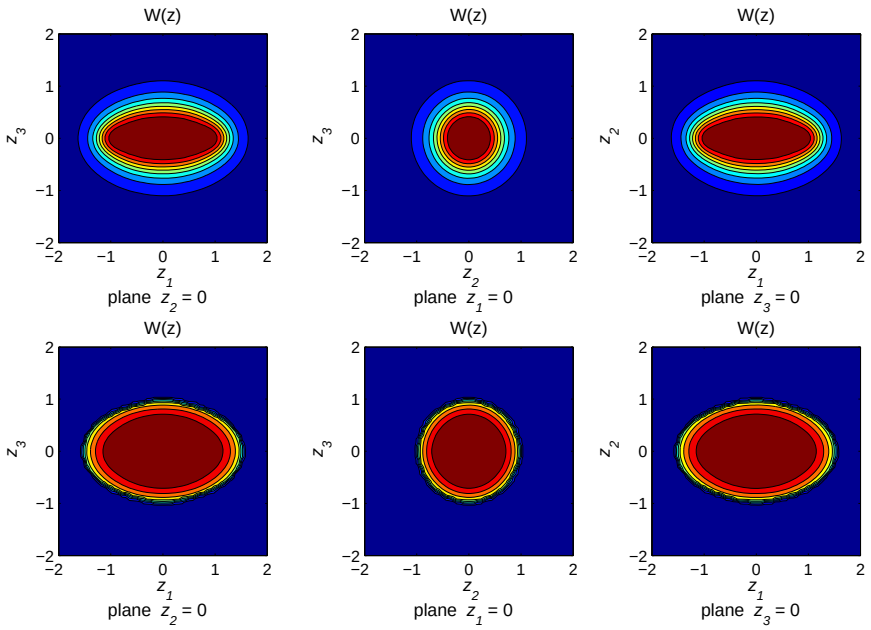

Figure 3: Isolines of $W(z)$ for GDP (top) and IMPC (bottom).

Figure 4 shows the surface $W(z)$, $z_3 = 0$ and isovalue parameters defined by (38)-(40) displayed as horizontal lines. The isovalue parameters are introduced in order to geometrically illustrate their role in the reconstruction process. Notice that for this example the level curves determined by each isovalue parameter not only give an excellent indicator of the shape of the object but also suggest that all the isovalue parameters will give good reconstructions in this particular case.

Figure 5 shows the reconstruction obtained by GDP and IMPC. Both methods yield very good reconstructions, however for GDP the exact noise level in F was used as input data.

Finally, in order to illustrate the convergence speed of IMPC algorithm, the number of iterations required for convergence in each grid point are displayed in a comprehensive way using a 3D plot, as seen in Figure 6 for the grid points corresponding to the plane $z_3 = 0$. For this example, the average number of iterations required for convergence was 29, with the observation that the largest number of iterations correspond to grid points near the boundary of the object.

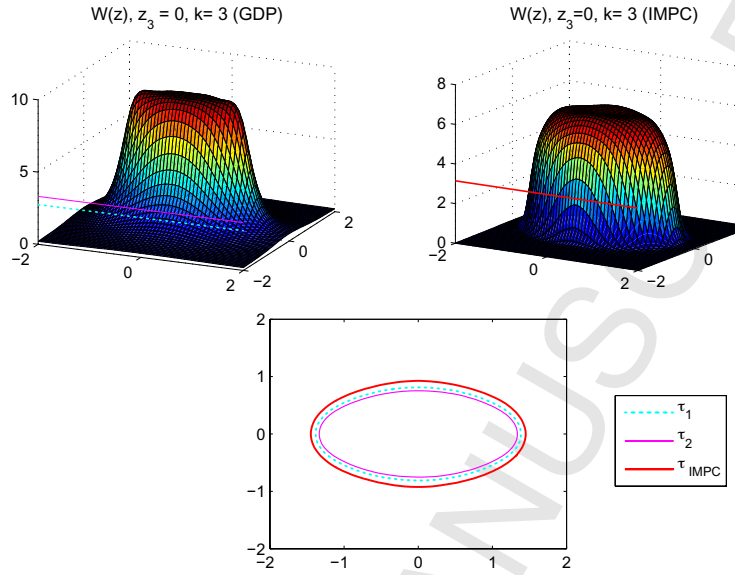

Figure 4: Top: Surface $W(z)$, $z_3 = 0$, and isovalue parameters displayed as horizontal lines. Bottom: Level curves of $W(z)$, $z_3 = 0$, determined by τ_1, τ_2 and τ_{IMPC}. In this example, $\tau_1 = 2.7515$ corresponds to $C = 0.3$, $\tau_2 = 3.3175$ and $\tau_{\text{IMPC}} = 3.1505$.

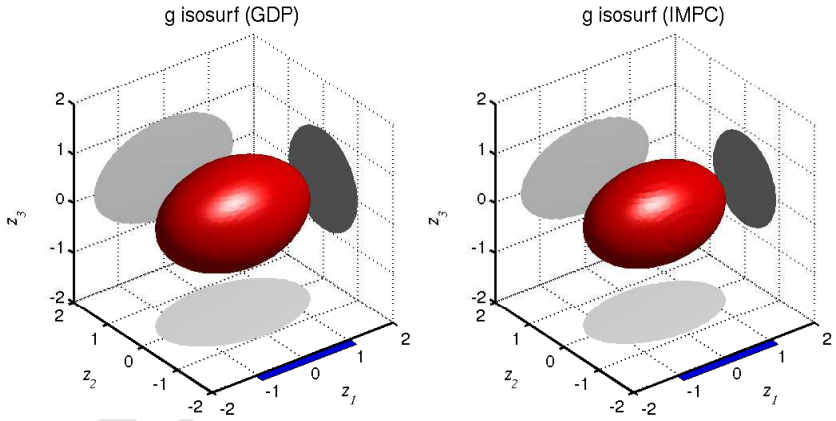

Figure 5: Reconstruction of an ellipsoid with index $n(x) = 2 + 2i$. The three-dimensional object and its projections on the planes (z_1, z_2), (z_2, z_3) and (z_1, z_3) are also shown.

4.2 Example 2: Two scatterers

We now describe numerical reconstructions of two spheres considering three cases as in [13].

a) Reconstruction of two homogeneous spheres with index $n(x) = 2 + 2i$.

We present the reconstructions obtained by GDP for two choices of the isovalue parameter τ_1 in order to illustrate why certain choices may not be appropriate. As in the previous example, we show the isolines of W for different cross sections (see Fig. 7) and see that they give a clear idea of

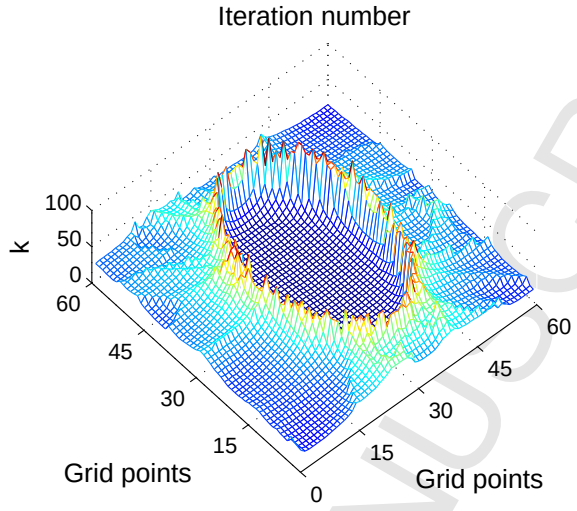

Figure 6: Iteration number required for convergence of IMP regarded as a surface defined on the 60×60 grid corresponding to $z_3 = 0$.

the shape of the objects.

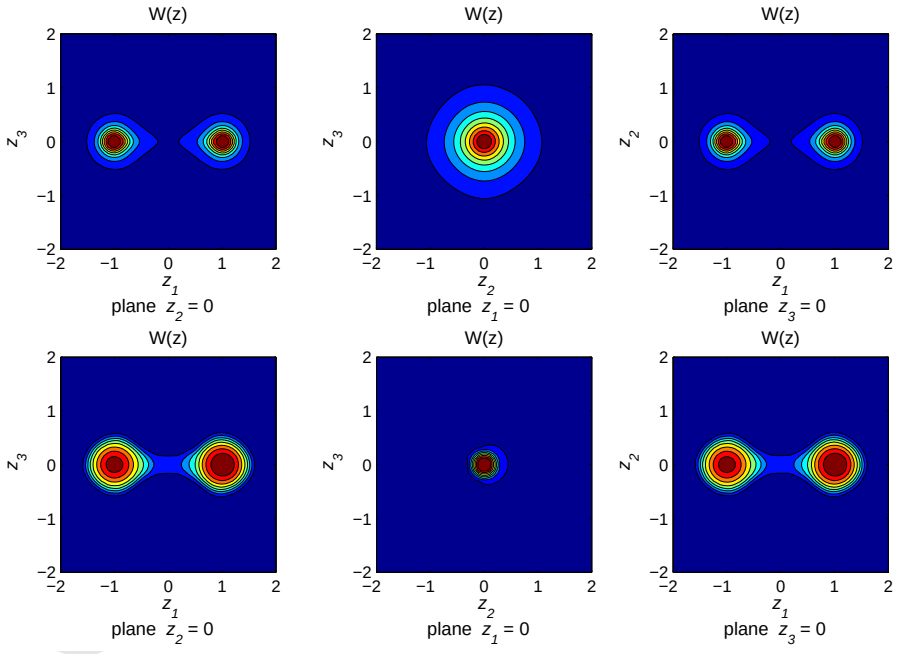

Figure 7: Isolines of $W(z)$ for GDP and IMPC. This example uses a noise level $\epsilon = 1\%$

Figure 8 shows the surface $W(z)$, $z_3 = 0$, isovalue parameters displayed as horizontal lines, and level curves determined by the parameters τ_1 (corresponding to $C = 0.1$) and τ_{IMPC} (corresponding to $\tau = 0.45$). The behavior of the level curves is critical to understand the role of the isovalue parameter in the reconstruction of the object. Of course, in spite of knowing that the shape of

the object is determined by the isolines, the point here is that the final result of the reconstruction depends on the cross section determined by the isovalue parameter. Taking this observation into account, it is apparent that, as in this case τ_1 is small, the cross section captures information associated to the object and information associated to the background, hence the reconstruction obtained by GDP with τ_1 as isovalue parameter should suffer some deformation. The same observation applies to the reconstructions obtained by GDP with τ_2. This is confirmed in Figure 9 (top), in which we present the reconstruction obtained by GDP with τ_1 corresponding to $C = 0.1$ as well as the reconstruction obtained by IMPC. To clarify the role of the parameter in the reconstruction, we also display in Figure 9 (bottom) the reconstruction obtained by GDP with τ_1 corresponding to $C = 0.3$. The results are now apparent. Again GDP was implemented with the exact noise level in F. Notice also that the IMPC reconstructions seem more accurate since the isovalue parameter does not capture information associated to the background.

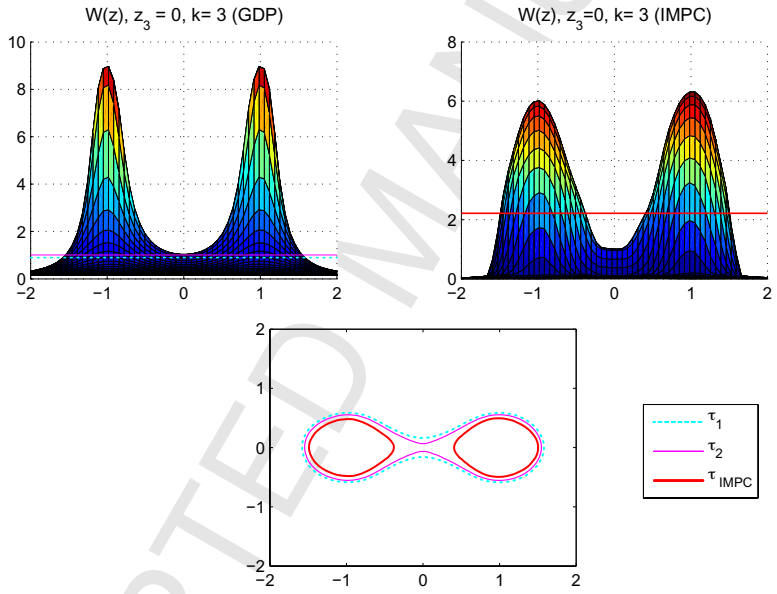

Figure 8: Surface $W(z)$, $z_3 = 0$, isovalue parameters displayed as horizontal lines, and level curves of $W(z)$, $z_3 = 0$, corresponding to the isovalue parameters.

b) Reconstruction of two spheres: one is absorbing and the other is non-absorbing.

This example deals with the case where the two media are different. To describe the results we show in Figure 10 the surface $W(z)$, $z_3 = 0$, isovalue parameters displayed as horizontal lines, and level curves determined by the parameters τ_1 corresponding to $C = 0.3$ and τ_{IMPC} corresponding to $\tau = 0.45$. Looking at the level curves, it is clear that while GDP with τ_1 and IMPC will produce good reconstructions, this will not be the case for GDP with τ_2. The reconstructions obtained by GDP and IMPC are shown in Figure 11. Another information that can be extracted from the level curves is that the volume of the object depends on the cross section area determined by the isovalue parameter. This explains why the balls obtained by GDP are slightly smaller than those determined by IMPC.

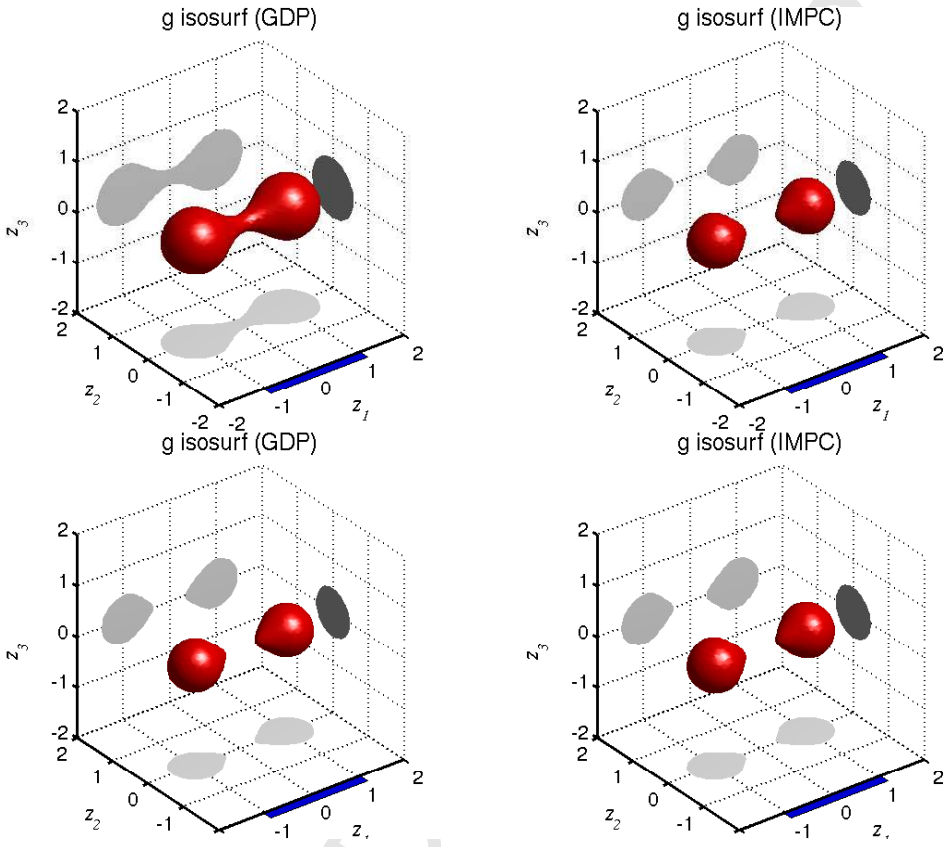

Figure 9: Reconstruction of two identical homogeneous spheres with index $n(x) = 2 + 2i$. Top $C = 0.1$, bottom $C = 0.3$.

c) Reconstruction of two spheres: one is absorbing and the other is a perfect conductor.

In this example we consider two noise levels: $\epsilon = 0.01$ and $\epsilon = 0.1$. The results of the reconstructions for the low noise level are shown in Figures 12 and 13. As in the example anterior, motivated by the behavior of the level curves, only the results obtained by GDP and IMPC are displayed. In this case, the GDP reconstruction corresponds to τ_1 with $C = 0.1$ (as done in [8]) and the IMPC reconstruction corresponds to $\tau = 0.45$. We notice that spheres reconstructed by GDP are deformed towards each other.

Finally, the results of the reconstructions for the high noise level ($\epsilon = 0.1$) are shown in Figure 14 (bottom) in which the surface $W(z), z_3 = 0$, and the isovalue parameters displayed as horizontal lines are also included. In this case, the GDP reconstruction correspond to $C = 0.35$ and the IMPC reconstruction corresponds to $\tau = 0.35$. The results show that LSM also works well in the case of data with high noise level.

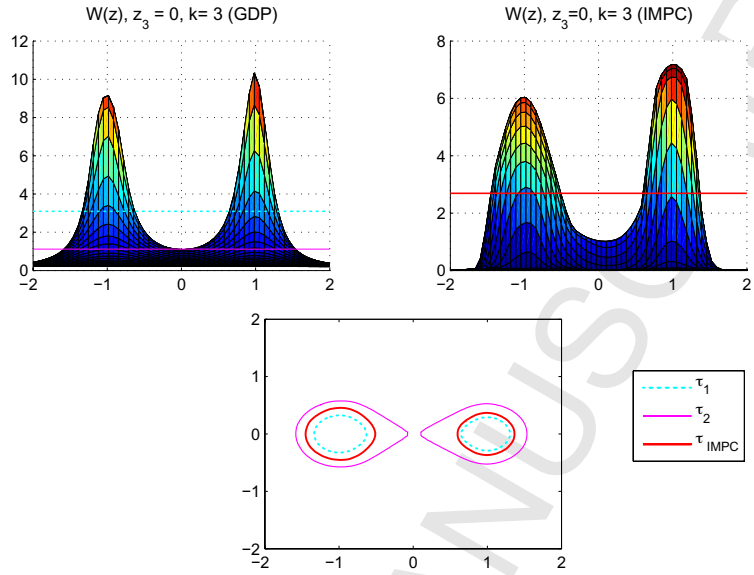

Figure 10: Surface $W(z)$, $z_3 = 0$, isovalue parameters displayed as horizontal lines and level curves of $W(z)$, $z_3 = 0$, corresponding to the isovalue parameters τ_1, τ_2 and τ_{IMPC}.

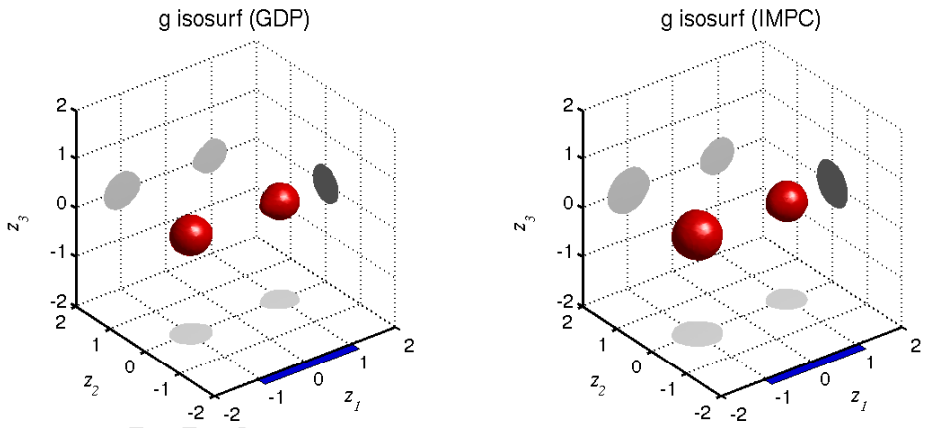

Figure 11: Reconstruction of two spheres where one is absorbing and the other one is non absorbing.

5 Conclusions

We have developed an improved maximum product criterion variant used to determine the regularization parameter for the linear sampling method applied to three dimensional penetrable scatterers. Our method is fast and efficiently selects as regularization parameter the largest local maximum of an appropriate product. In addition, we discussed the selection of the isovalue parameter for visualizing the scatter and proposed a heuristic for such selection that was numerically proved efficient. The quality of reconstructions is comparable to the ones obtained via Morozov's discrepancy principle where the noise level is known *a priori*. The IMPC however does not require

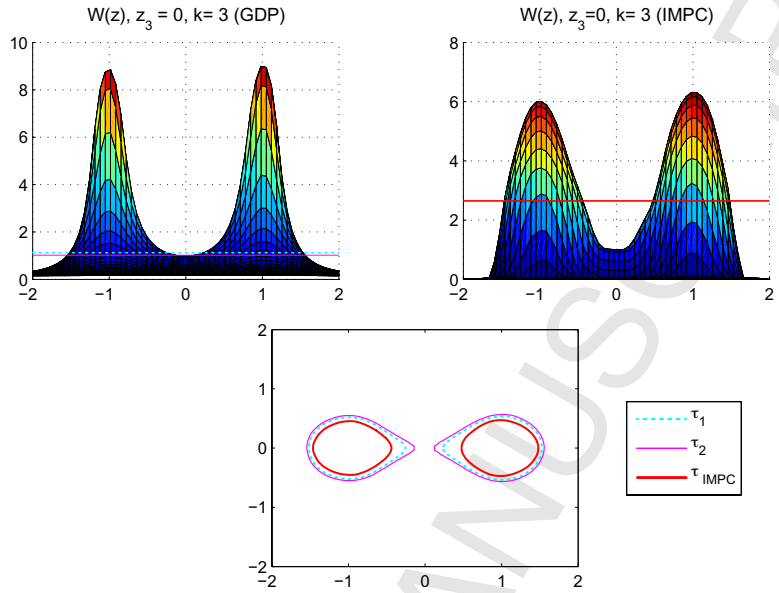

Figure 12: Surface $W(z)$, $z_3 = 0$, isovalue parameters displayed as horizontal lines. Bottom: Level curves of $W(z)$, $z_3 = 0$, corresponding to the isovalue parameters τ_1, τ_2 and τ_{IMPC}.

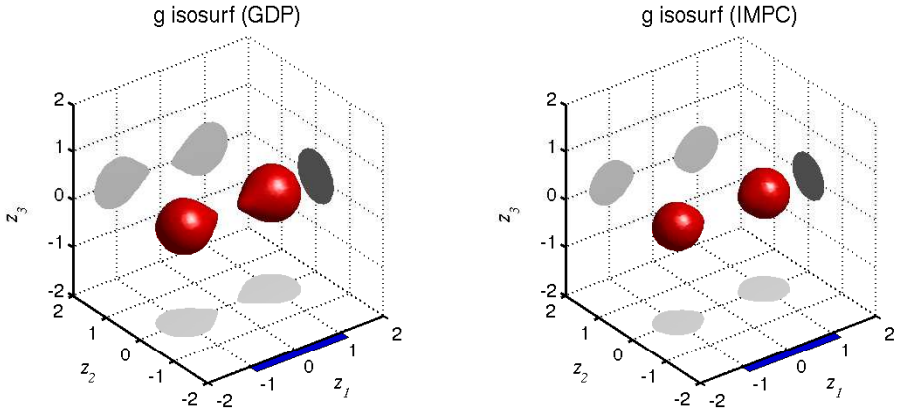

Figure 13: Reconstruction of two spheres where one is absorbing and the other is a perfect conductor.

a priori knowledge of the noise level, a situation which is very likely in real world problems.

6 Acknowledgements

The authors would like to thank Professor Monk for his valuable help with the construction of the computer code and Professor Fares for kindly providing them with the three dimensional direct data.

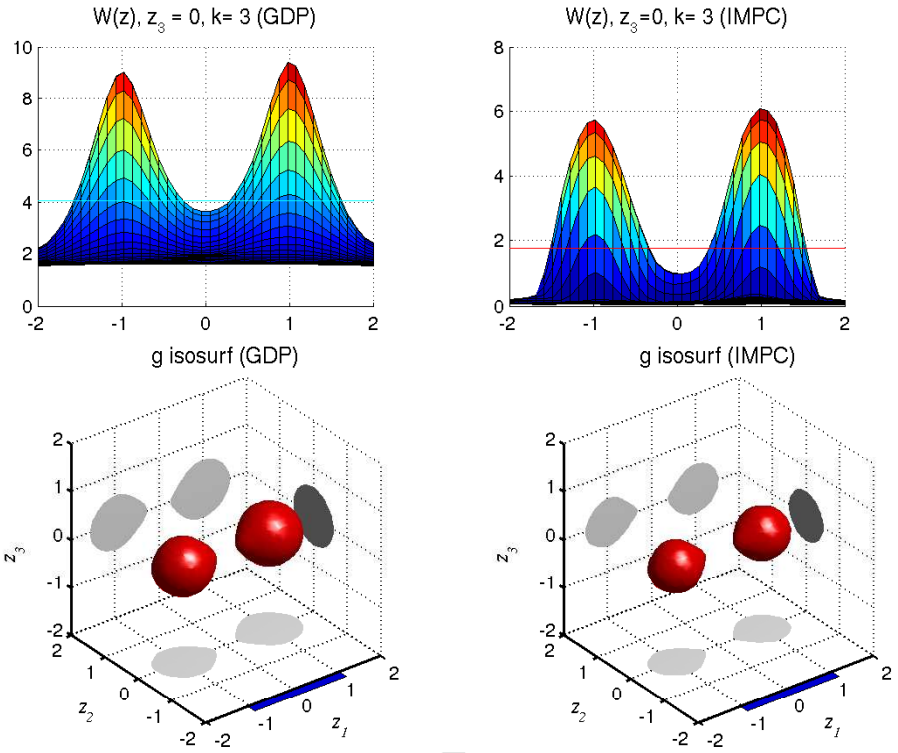

Figure 14: Top: Surface $W(z), z_3 = 0$, and isovalue parameters displayed as horizontal lines. Bottom Reconstruction of two spheres where one is absorbing and the other is a perfect conductor.

References

[1] Aramini R, Brignone M and Piana M 2006 The linear sampling method without sampling *inverse problems* **22** 2237-54

[2] Bazán F S 2008 Fixed-point iterations in determining the Tikhonov regularization parameter *Inverse Problems* **24** 1-15

[3] Bazán F S and Francisco J B 2009 An improved Fixed-point algorithm for determining a Tikhonov regularization parameter *Inverse Problems* **25**

[4] Bazán F S, Francisco J B, K H Leem, and Pelekanos G 2012, A maximum product criterion as a Tikhonov parameter choice rule for Kirsch's factorization method J. Comp. Appl. Math. 236, 4264-4275.

[5] Colton D and Kirsch A 1996 A simple method for solving the inverse scattering problems in the resonance region *Inverse Problems* **12** 383-393

[6] Colton D and Kress R 1998 *Inverse Acoustic and Electromagnetic Scattering Theory, 2nd edn.* (New York:Springer-Verlag),

[7] Colton D, Piana M and Potthast R 1999 A simple method using Morozov's discrepancy principle for solving inverse scattering problems *Inverse Problems* **13** 1477-93

[8] Colton D, Haddar H and Piana M 2003 The linear sampling method in inverse electromagnetic scattering theory *Inverse Problems* **19** 105-137

[9] Collino F, Fares M and Haddar H 2003 Numerical and analytical studies of the linear sampling method in electromagnetic inverse scattering problems, *Inverse Problems* 19 1279-1298.

[10] Colton D, Haddar H and Monk P 2003 The linear sampling method for solving the electromagnetic inverse scattering problem *Siam J. Sci. Comput.* **24(3)** 719-731.

[11] Fares M, Gratton S, Toint P 2011 Fast regularized linear sampling for inverse scattering problems *Numerical Linear Algebra with Applications*, 18(1) 55-68.

[12] Fares M, Gratton S, Toint P 2009 SVD-tail: a new linear-sampling reconstruction method for inverse scattering problems, *Inverse Problems* 25 1-19.

[13] Haddar H and Monk P 2002 The linear sampling method for solving the electromagnetic inverse medium problem *Inverse Problems* **18** 891-906.

[14] P. C. Hansen, Rank-Deficient and Discrete Ill-Posed Problems, SIAM, Philadelphia, 1998.

[15] Kirsch A 1998 Characterization of the shape of a scattering obstacle using the spectral data of the far field operator *Inverse Problems* **14** 1489-1512.

[16] Kress R 2001 *Electromagnetic waves scattering.* New York: Academic

[17] K. H. Leem K H, G. Pelekanos G Bazán F S 2010 Fixed-point iterations in determining a Tikhonov regularization parameter in Kirsch's factorization method, Applied Math. Comput. 216 3747-3753.

[18] Pelekanos G and Sevroglou V 2006 Shape reconstruction of a 2D-elastic penetrable object via the L-curve method, J. Inv. Ill-Posed Problems 14 1-16.